

Synchronization time in a hyperbolic dynamical system with long-range interactions

Rodrigo F. Pereira^a, Sandro E. de S. Pinto^{a,*}, Sergio R. Lopes^b

^a*Departamento de Física, Universidade Estadual de Ponta Grossa, 84030-900, Ponta Grossa, PR, Brazil*

^b*Departamento de Física, Universidade Federal do Paraná, 81531-990, Curitiba, PR, Brazil*

Abstract

We show that the threshold of complete synchronization in a lattice of coupled non-smooth chaotic maps is determined by linear stability along the directions transversal to the synchronization subspace. We examine carefully the synchronization time and show that an inadequate observation of the system evolution leads to wrong results. We present both careful numerical experiments and a rigorous mathematical explanation confirming this fact, allowing for a generalization involving hyperbolic coupled map lattices.

Keywords: coupled map lattices, long-range interactions, synchronization time

PACS: 05.45.Xt, 05.45.Pq, 05.45.Ra

1 The possibility of synchronizing chaotic dynamics has been harnessed in
2 a large number of systems of physical interest [1, 2], like coupled Josephson
3 junctions [3] and lasers [4]. Although there have been identified different

*Corresponding author

Email addresses: pereira.rf@gmail.com (Rodrigo F. Pereira),
desouzapinto@pq.cnpq.br (Sandro E. de S. Pinto)

4 types of chaos synchronization, we shall concentrate on the so-called ampli-
5 tude or complete synchronization, for which all dynamical variables undergo
6 the same time evolution [5]. The essential dynamics involved in the process
7 of chaos synchronization lies on the low-dimensionality of the subspace (in
8 the phase space of the system) in which synchronized motion sets in.

9 For example, if we consider a lattice of N coupled oscillators, each of
10 them represented by a vector field of D dimensions, where typically $D \ll N$,
11 the synchronized state belongs to a D -dimensional subspace of the ND -
12 dimensional phase space. In order for this synchronized state to exist the
13 coupling among oscillators takes on a suitable form [6]. Whether or not this
14 synchronized state is stable, however, is a more difficult question, since it in-
15 volves the analysis of infinitesimal displacements from the synchronized state
16 along all $(N - 1)D$ directions transversal to the synchronization subspace [7].
17 The stability condition of the synchronized orbit with respect to transversal
18 perturbations can be obtained from the negativeness of the largest transversal
19 Lyapunov exponent.

20 In this paper we consider a coupled chaotic map lattice (CML) in which
21 the coupling prescription is linear and non-local, for it takes into account the
22 distance between maps along the lattice. Such non-local couplings appear in
23 many problems of physical [8] and biological interest [9]. We suppose that the
24 coupling strength decreases with the lattice distance as a power-law, which
25 characteristic exponent can take on any non-negative value [10]. The loss
26 of transversal stability of the synchronized state, as the coupling parameters
27 are varied, was found in such power-law couplings, with help of the largest
28 transversal Lyapunov exponent, for a number of chaotic maps [11, 12]. In

29 the particular case of maps with constant eigenvalues of the Jacobian matrix
 30 (piecewise-linear chaotic maps) we obtained analytical results for the loss of
 31 transversal stability of the synchronized state which agree with the numer-
 32 ical simulations [13]. Such CML's represent hyperbolic dynamical systems
 33 (see text below), what enables us to use powerful mathematical tools like
 34 ergodicity and global shadowing of numerically generated orbits [14].

35 On the other hand, in a recent paper there was argued that in the special
 36 case of coupled non-smooth discontinuous maps the synchronization transi-
 37 tion would not be given by the largest transversal exponent, but rather by
 38 a different approach taking into account finite distances from the synchro-
 39 nized state [15]. To investigate this apparent contradiction we considered in
 40 this paper the transient behavior of the non-synchronized orbits for coupled
 41 piecewise linear maps. Our results show that the analytical results of Ref.
 42 [13] (using linear transversal stability of the synchronized state) *hold for both*
 43 *smooth and non-smooth maps*, the numerical results being strongly affected
 44 by many factors as the large transient time and the choice of initial condi-
 45 tions. Due to these factors, the time it takes to achieve convergence to the
 46 synchronized state may be extremely large, what may lead to wrong conclu-
 47 sions about the stationary state of the system. Motivated by this problem,
 48 we investigated the validity of the transversal linear stability analysis in a
 49 class of hyperbolic CML's, using periodic-orbit theory to unveil the role of
 50 the unstable orbits embedded in the synchronized state [16–18].

51 The CML we consider in this work can be written in the explicit form of
 52 a N -dimensional dynamical system

$$\mathbf{x}_{n+1} = (\mathbf{1} + \mathbf{C})\mathbf{F}(\mathbf{x}_n) \equiv \mathbf{B}\mathbf{F}(\mathbf{x}_n), \quad (1)$$

53 where the components of $\mathbf{x}_n = (x_n^{(1)}, x_n^{(2)}, \dots, x_n^{(N)})^T$ denote the state vari-
 54 able attached to the map located at the site $i = 1, \dots, N$ at time $n =$
 55 $0, 1, \dots$. If the uncoupled maps are written as $x \mapsto f(x)$ we can write
 56 $\mathbf{F}(\mathbf{x}) = [f(x^{(1)}), f(x^{(2)}), \dots, f(x^{(N)})]^T$. Moreover, the coupling prescription
 57 is represented by the matrix \mathbf{C} , and $\mathbf{1}$ is the identity matrix.

58 In the following we consider the generalized Bernoulli map $f(x) = \beta x,$
 59 $(\text{mod } 1)$, where $x \in [0, 1)$ and $\beta > 1$, such that the isolated map generates
 60 a strongly chaotic orbit. When these piecewise-linear maps are coupled ac-
 61 cording to Eq. (1), in order to ensure that $x_n^{(i)} \in [0, 1)$, the elements of \mathbf{B}
 62 must satisfy the following necessary and sufficient conditions: $B_{ij} \geq 0$, and
 63 $0 \leq \sum_{j=1}^N B_{ij} \leq 1$, for all $i, j = 1, 2, \dots, N$ [19]. Moreover, we use a symmetric
 64 coupling matrix with elements

$$C_{ij} = \varepsilon \eta^{-1} [r_{ij}^{-\alpha} (1 - \delta_{ij}) - \eta \delta_{ij}], \quad (2)$$

65 where $r_{ij} = \min_{l \in \mathbb{Z}} |i - j + lN|$ is the minimum lattice distance between
 66 the sites i and j (with periodic boundary conditions), $\eta = 2 \sum_1^{N'} r^{-\alpha}$, with
 67 $N' = (N - 1)/2$ (which requires N odd), and the coupling strength satisfies
 68 $0 \leq \varepsilon \leq 1$ due to the constraints on B_{ij} . The effective range of interactions
 69 is represented by $\alpha \geq 0$ such that the limits $\alpha = 0$ and $\alpha \rightarrow \infty$ correspond,
 70 respectively, to global (mean field) and local (first neighbors) coupling pre-
 71 scriptions.

A completely synchronized state is the chaotic orbit for which $x_n^{(1)} = \dots =$
 $x_n^{(N)}$, and which is a solution of Eq. (1). Since the Jacobian $\mathbf{DF} = \beta \mathbf{B}$ is a
 circulant matrix, its eigenvalues can be analytically obtained as

$$\Lambda^{(k)} = \beta [(1 - \varepsilon) + (\varepsilon/\eta) b^{(k-1)}],$$

72 where

$$b^{(k)} = \sum_{m=1}^{N'} \frac{1}{m^\alpha} \cos\left(\frac{2\pi km}{N}\right), \quad (0 \leq k < N) \quad (3)$$

73 such that the Lyapunov spectrum $\{\lambda_i\}_{i=1}^N$ can be derived [13]. The stability
 74 threshold of the synchronized state with respect to infinitesimal transver-
 75 sal displacements, obtained by imposing $\lambda_2 = 0$, gives two curves in the
 76 parameter plane (ε versus α): (i) $\varepsilon'_c(\alpha, N) = \min\{\varepsilon_{up}(\alpha, N), 1\}$; and (ii)
 77 $\varepsilon_c(\alpha, N) = \min\{\varepsilon_{lo}(\alpha, N), 1\}$, where we defined

$$\varepsilon_{up}(\alpha, N) = (1 + \beta^{-1})[1 - (b^{(N')}/\eta)]^{-1}, \quad (4)$$

$$\varepsilon_{lo}(\alpha, N) = (1 - \beta^{-1})[1 - (b^{(1)}/\eta)]^{-1}. \quad (5)$$

78 In order to check the validity of these analytical conditions for the thresh-
 79 old of transversal stability we have made careful numerical experiments using
 80 the same criteria as proposed in Ref. [15] (where it has been claimed that
 81 those conditions would hold only for coupled continuous maps). Accordingly,
 82 we choose initial conditions $x_0^{(i)}$ uniformly distributed in the interval $[0, 1]$ ¹.
 83 The CML is firstly iterated for a transient time of $T_w = 10^w \times N$ times and
 84 further iterated by more $T = 10^3 \times N$ times. As a numerical diagnostic of
 85 complete synchronization we computed the following quantity

$$R = \sum_{n,i} \frac{1}{NT} \left| x_n^{(i)} - \left(\frac{1}{N} \sum_j x_n^{(j)} \right) \right|, \quad (6)$$

86 which is essentially a mean deviation from the lattice-averaged amplitude.
 87 The resulting dynamical state is considered as being completely synchro-
 88 nized if $R < 10^{-8}$. In the coupling parameter space we keep α constant

¹We initialized the random number generator `ran1` from Ref. [20] with always the same the seed (-28937104)

89 and sweep through the values of $\varepsilon \in [0, 1]$. The value corresponding to the
90 synchronization threshold, denoted as ε_{num} , is obtained from bisection as
91 $\varepsilon_{num} = (\varepsilon_s + \varepsilon_d)/2$, where ε_s and ε_d are, respectively, the last value corre-
92 sponding to a synchronized state and the first value for a non-synchronized
93 one. The numerical value of ε_{num} is turned more accurate from refining the
94 increment mesh and repeating the process, until $(\varepsilon_s - \varepsilon_d) \leq 10^{-3}$.

95 The results of this numerical procedure, for the case $\beta = 1.1$, are de-
96 picted in Figure 1, where we show the value of the coupling strength at the
97 synchronization threshold as a function of α . In Fig. 1(a) we show how the
98 numerically determined critical value increases with α for different lattice
99 sizes N , the transient time being different for each choice, using $w = 5$. The
100 solid lines correspond to the analytical condition derived in Ref.[13] (and that
101 depend on the lattice size as well). In fact, as the lattice size N increases,
102 the numerical values of ε_{num} may no longer match the analytically predicted
103 values, if α is large enough [15]. This does not mean, however, that the an-
104 alytical value of ε_c is not valid in those cases, but rather that *the numerical*
105 *simulations have not been performed using a transient long enough*. To show
106 the influence of the transient time in the results, we show in Fig. 1(b) the
107 dependence of ε_{num} with α for a fixed lattice of $N = 129$ sites by changing
108 the parameter w . By increasing the transient time the numerically obtained
109 values for the synchronization threshold agree better with those derived from
110 transversal linear stability. The same conclusions were obtained using other
111 lattice sizes as well. These results suggest that the analytical result for ε_c
112 remains valid, as long as we use sufficiently long transient times, in contrast
113 with Ref. [15].

114 Another factor that affects the accuracy of numerical results for the
 115 threshold of synchronization is that a distribution of initial conditions over
 116 the interval $[0, 1)$ should respect the natural measure of the chaotic orbit,
 117 because we are assuming the coupling between typical oscillators, which are
 118 characterized by trajectories in the steady-state system, *i. e.*, trajectories
 119 that satisfy the invariant density of the system. While for integer values of
 120 β the natural measure is uniform, this is no longer valid for fractional β ,
 121 and small errors may be introduced if we choose initial conditions with a
 122 uniform probability distribution. In order to overcome this problem we iter-
 123 ated each map s times before starting coupling them according to Eq. (1)
 124 (this transient time should not be confused with the transient time T_w we
 125 compute after having started coupling the maps). In Figure 1(c) we com-
 126 pare the results of two simulations: for the line with filled triangles we used
 127 initial conditions uniformly distributed along $[0, 1)$, without discarding any
 128 transients ($s = 0$); whereas the line with open triangles was obtained from
 129 initial conditions chosen with respect to a numerical approximation of the
 130 natural measure, the latter having being obtained from a transient time of
 131 $s = 10^4$ iterations. The results obeying the natural measure of the uncoupled
 132 oscillators are more likely to agree with the analytical results since, after the
 133 synchronized state sets in, the corresponding orbit must follow this natural
 134 measure. As will be formally discussed below, in the limit $n \rightarrow \infty$, the results
 135 are independent of the (typical) initial distribution of trajectories. But for fi-
 136 nite time intervals, time synchronization can depend on such distribution.
 137 This dependence is due to local dynamics and form of coupling.

138 In order to analyze the dependence of ε_{num} on the initial conditions, we

139 performed extensive numerical simulations with an ensemble of 5000 identi-
 140 cally prepared CML's, each of them with a different initial condition [Fig.
 141 1(d)] and the same transient time ($w = 5$). We observed different values of
 142 ε_{num} for each initial condition, provided α is large enough. Instead of showing
 143 each of them (what would turn the figure too much loaded with symbols) we
 144 represented in Fig. 1(d) only those numerical values of ε_{num} that are closest
 145 (open circles) and farthest (filled circles) with respect to the analytical value
 146 (full line). Note that synchronization of one typical trajectory implies global
 147 stability of the synchronized state, since the system is hyperbolic. A chaotic
 148 invariant set Ω is hyperbolic if the following conditions are fulfilled: (i) the
 149 tangent space at each point $\mathbf{x} \in \Omega$ can be decomposed in two invariant sub-
 150 spaces (a stable and an unstable one) with constant dimensions; (ii) these
 151 subspaces always intersect transversely (i.e., they cannot present tangencies);
 152 and (iii) this decomposition is consistent under the dynamics in Ω generated
 153 by \mathbf{F} [14]. For coupled generalized Bernoulli maps the set Ω is the N -torus
 154 $[0, 1)^N$ and the Jacobian matrix \mathbf{DF} has constant entries and does not de-
 155 pend on $\mathbf{x} \in \Omega$, thus the dimension of the invariant subspaces is constant
 156 everywhere [condition (i)]. Thanks to this particular form of the Jacobian its
 157 eigenvectors (which span the invariant subspaces) are everywhere orthogonal
 158 [condition (ii)]. Let \mathbf{u} be any of such eigenvectors: under the dynamics of \mathbf{F}
 159 it follows that \mathbf{u} is mapped to a vector along the same direction [condition
 160 (iii)]. Hence the set Ω is a hyperbolic structure for \mathbf{F} .

It is possible to understand, from a general point of view, the causes of the
 strong dependence of the synchronization threshold results on the transient
 time and the initial conditions. These causes are not restricted to coupled

161 piecewise-linear maps as ours, but are rather generic for hyperbolic CML's.
 162 We can extend our conclusions to a CML given by Eq. (1) where the coupling
 163 prescription keeps invariant the phase space $\Omega = [0, 1)^N$, and for which

$$\mathcal{S} = \{\mathbf{x} \in \Omega : x^{(1)} = \dots = x^{(N)}\}$$

164 is the one-dimensional invariant synchronization manifold defined by the cor-
 165 responding state. We consider a Δ -neighborhood of \mathcal{S} as the set of points
 166 whose distances from the \mathcal{S} do not exceed Δ : $\Sigma_\Delta = \{\mathbf{x} : d(\mathbf{x}, \mathcal{S}) \leq \Delta\}$,
 167 where d is a suitably defined distance on the metric space Ω . We define
 168 $\Sigma \equiv \lim_{\Delta \rightarrow 0} \Sigma_\Delta$ as a linear neighborhood of \mathcal{S} . Accordingly $\Gamma = \Omega - \Sigma$ is the
 169 phase space region, except the linear neighborhood of the synchronization
 170 manifold.

171 We can speak of the global dynamics generated by the coupled map lattice
 172 $\mathbf{x}_{n+1} = \mathbf{BF}(\mathbf{x}_n)$ in terms of their periodic points. In this spirit we denote
 173 $\mathbf{x}_j(p)$ the j th fixed point of the p -times iterated vector function $\mathbf{BF}(\mathbf{x}_n)$. The
 174 i th eigenvalue of the Jacobian matrix of $\mathbf{BF}^{[p]}(\mathbf{x}_n)$, evaluated at this point,
 175 is written as $\Lambda_i(\mathbf{x}_j(p))$, such that $|\Lambda_1(\mathbf{x}_j(p))| \geq \dots \geq |\Lambda_N(\mathbf{x}_j(p))|$.

176 Let us consider a subset of the phase space, $A \subset \Omega$, with natural measure
 177 $\mu(A)$. Note that, by construction, we have $\mu(\Omega) = 1$. For hyperbolic systems
 178 satisfying the Axiom-A ² the natural measure of such subset can be obtained
 179 from the unstable periodic points embedded in it as [16]

$$\mu(A) = \lim_{p \rightarrow \infty} \sum 1/L_j(p), \quad (7)$$

²A hyperbolic system satisfying Axiom-A must be also mixing. This condition is fulfilled if the system possesses a dense set of unstable periodic orbits embedded in the phase space [14].

177 where $L_j(p) = \prod_{i=1}^{d_u} |\Lambda_i(\mathbf{x}_j(p))|$ (d_u is the largest integer such that $|\Lambda_{d_u}(\mathbf{x}_j(p))| >$
 178 1) and the sum sweeps over all $\mathbf{x}_j(p) \in A$. The exploitation of this iden-
 179 tity is the object of periodic-orbit theory, that has been used for a number
 180 of theoretical investigations on the properties of chaotic dynamical systems
 181 [17, 18]. For generalized Bernoulli maps $\beta x \pmod{1}$ and a linear coupling,
 182 the Jacobian matrix has constant entries and thus do not depend on the
 183 orbit points, *i.e.*, all the unstable periodic orbits have the same eigenvalue
 184 spectra (consequently $L_j(p) = L(p)$ for all j), and the natural measure is
 185 $\mu(A) = \lim_{p \rightarrow \infty} N_A(p)/L(p)$, where $N_A(p)$ is the number of period- p points
 186 contained in the subset A of Ω .

187 A byproduct of the periodic-orbit theory is that the (linear) transversal
 188 stability of the synchronization manifold can be studied either from the nat-
 189 ural measure of a typical chaotic orbit (by the second largest Lyapunov expo-
 190 nent) or from the atypical measure generated by the unstable periodic orbits.
 191 In particular, with respect to the period- p orbit the threshold of transversal
 192 stability of the synchronization manifold can be obtained from the condition
 193 $|\Lambda_2(\mathbf{x}_j(p))| = 1$ for all $\mathbf{x}_j(p) \in \mathcal{S}$. As the period p goes to infinity we expect
 194 an increasingly better agreement of this result with that obtained by using
 195 the second largest transversal Lyapunov exponent (or $\lambda_2 = 0$). For a given
 196 α and values of the coupling strengths such that $\varepsilon_{lo}(\alpha) < \varepsilon < \varepsilon_{up}(\alpha)$, the
 197 natural measure of the subset A is

$$\mu(A) = \lim_{p \rightarrow \infty} N_A(p)/\beta^p. \quad (8)$$

198 Taking A to be the linear neighborhood of the synchronization manifold,
 199 Σ , there follows that the number of orbits in this neighborhood is $N_\Sigma = \beta^p - 1$
 200 for integer β (if β is fractional, as in the numerical simulations of the previous

201 section, $N_p \rightarrow \beta^p$ for $p \gg 1$) and the corresponding natural measure is given
 202 by

$$\mu(\Sigma) = \lim_{p \rightarrow \infty} (\beta^p - 1)\beta^{-p} = 1, \quad (9)$$

203 demonstrating that the linear neighborhood of the synchronization manifold
 204 \mathcal{S} is the asymptotic state of any typical initial condition (in the sense that the
 205 set of initial conditions that do not converge to Σ has zero Lebesgue measure).
 206 This result is obtained for the parameter regime in which the synchronized
 207 state is locally stable and, therefore, any trajectory in Σ converges exponen-
 208 tially to \mathcal{S} at a rate $\lambda_2 < 0$. An immediate consequence of this result is that
 209 the natural measure outside the linear neighborhood is zero since, using the
 210 fact that the natural measure is ergodic, we have $\mu(\Gamma) = \mu(\Omega) - \mu(\Sigma) = 0$.

211 Given that almost all initial conditions outside the synchronization man-
 212 ifold eventually asymptote to it, we may well ask why sometimes it takes so
 213 long for this convergence to be observed in numerical experiments. As we
 214 saw previously, this long transient time may even be mistaken as a effect
 215 of non-convergence. The answer lies in the properties of the horseshoe-like
 216 invariant chaotic set embedded in Γ . This set is non-attracting since almost
 217 all initial conditions in Γ converge to \mathcal{S} as the time goes to infinity.

218 Let $\tilde{\rho}_n(\mathbf{x})$ be the density of trajectories around \mathbf{x} at time n , so that

$$\mu(A) = \lim_{n \rightarrow \infty} \int_A \tilde{\rho}_n(\mathbf{x}) d\mathbf{x} \quad (10)$$

219 for any typical $\tilde{\rho}_0(\mathbf{x})$. The above result is independent of the specific form
 220 of $\tilde{\rho}_0$ in the limit $n \rightarrow \infty$. The possibility of expanding $\tilde{\rho}_0$ in terms of the
 221 eigenfunctions of the Perron-Frobenius operator justifies such independence
 222 of $\mu(A)$, since the invariant density $\rho(\mathbf{x})$ of the system is associated with the

223 largest eigenvalue (which is not degenerate) of that operator [21]. Note that
 224 for finite time intervals, the convergence of the invariant density depends on
 225 the coefficients of expansion of $\tilde{\rho}_0(\mathbf{x})$ on the basis of eigenfunctions of the
 226 Perron-Frobenius operator. The results in Figure 1(c) are evidence of the
 227 assertion of the previous sentence.

228 However, the measure generated by chaotic orbits whose initial conditions
 229 are uniformly distributed over of an open region B of the phase space Ω
 230 decays exponentially with time with escape rate γ ,

$$\int_B \tilde{\rho}_{n+m}(\mathbf{x}) d\mathbf{x} = e^{-\gamma n} \int_B \tilde{\rho}_m(\mathbf{x}) d\mathbf{x} \quad (11)$$

231 with $m \gg 1$. For hyperbolic systems it can be shown that the escape rate is
 232 also obtained in terms of unstable periodic points of the saddle according to

$$\lim_{p \rightarrow \infty} e^{-\gamma p} \sum_{\mathbf{x}_j(p) \in B} 1/L_j(p) = 1, \quad (12)$$

233 where in the sum we consider only the periodic orbits of the horseshoe-like
 234 set B outside the synchronization manifold [16]. Hence, if one picks up at
 235 random an initial condition off the synchronization manifold, the distribu-
 236 tion of the transient times is likely to be exponential, with a characteristic
 237 exponent dependent on the escape rate γ . This is illustrated in Figure 2,
 238 in which the distribution of synchronization times (transient time intervals),
 239 $\phi(n)$, is indicated for a typical realization of the network, with $N = 17$.
 240 Figure 2 also points out a numerical estimate of the density measure de-
 241 cay of the unsynchronized state. To obtain this estimate, we cover Γ with
 242 K_0 uniformly distributed initial conditions and, at each time instant n , we
 243 count the number K_n of trajectories that remain in Γ under the system

244 evolution. The temporal decay of K_n provides the escape rate of Γ since
 245 $K_n/K_0 \approx \int_{\Gamma} \tilde{\rho}_n(\mathbf{x}) d\mathbf{x}$, for $K_0 \gg 1$. Note that the exponential decay of the
 246 curves is the same in Figure 2. The mean time of synchronization (or the
 247 mean life of the chaotic saddle), given by

$$\langle n \rangle = \int_0^{\infty} n \phi(n) dn \approx \frac{1}{\gamma}, \quad (13)$$

248 is indicated by a red arrow on the x -axis. The rightmost term in Eq. (13)
 249 is obtained by supposing $\phi(n) \propto e^{-\gamma n}$ – which is typical for chaotic saddles
 250 and is verified in Fig. 2.

251 If the initial condition is too close to an unstable periodic orbit (or its
 252 stable manifold) of B it would stick to it for some time-span and hence it
 253 takes a very long time for such a trajectory to approach the synchronization
 254 manifold, as illustrated in Fig. 3. This seems to occur very often if we use
 255 fractional values of β , like in the numerical simulations we shown in this
 256 paper.

257 We show in Figure 3 a situation in which the trajectory escapes from
 258 the neighborhood of an orbit with small period (~ 30), and instantly ac-
 259 cess the synchronized state. However, since there is a chaotic saddle in Γ ,
 260 there is a dense set of unstable periodic points in the unsynchronized state,
 261 and a trajectory can wander between different UPO's before escaping to the
 262 synchronized state.

263 To demonstrate that the behavior shown in Figure 2 is typical, we present
 264 in Figure 4 two numerical estimates for the invariant density of the chaotic
 265 saddle in the unsynchronized state. In Figure 4(a), which is obtained from
 266 typical trajectories, the invariant density is shown in a projection on the
 267 $x^{(i)} \times x^{(i+1)}$ plane (due to symmetry the network, the value of i is irrelevant).

268 The most visited regions in that figure are represented by symbols whose
 269 color is dark blue and the least visited by light green symbols. The estimate
 270 for the density in terms of UPO's is shown in Figure 4(b). For this case, all
 271 the unstable orbits with the period less than or equal to 35 are considered.
 272 Comparing the two figures is apparent that the structures in Figure 4(a)
 273 are supported by the orbits in Figure 4(b). The processing time was the
 274 limiting factor for choosing the value of the period in the simulations shown
 275 in Fig. 4(b)³. The Table 1 shows the mean differences between the values
 276 of projections of $\rho(\mathbf{x})$ and $\rho_p(\mathbf{x})$, the density values obtained by calculation
 277 of all points in Γ with period $q \leq p$. This calculation was done in a grid of
 278 128×128 boxes, each one as the same size. We also found that the average
 279 difference decreases as the period increases, this is according to reference [22].
 280 When the period tends to infinity, we obtain the exact measure of the saddle
 281 [16].

282 From the view of the structure of the chaotic saddle provided by Figure 4,
 283 it is easy to understand how the distribution of initial conditions affects the
 284 results for simulations with finite time. For the case we are considering, the
 285 Bernoulli map with $\beta = 1.10$, the density of the natural measure in the unit
 286 interval is mainly concentrated near zero. In Figure 4(b) the chaotic saddle
 287 is less dense at the bottom left than in the upper right corner, *i.e.*, the initial
 288 conditions close to zero spend less time to synchronize. However, it should
 289 be noted that this dependence with the initial distribution of trajectories is a
 290 consequence of the finite time simulations because, as shown, such as effects

³For $p = 28$ there are around 10000 periodic points in Γ . However, for $p = 35$ there are
 around 10000000 points.

Period p	$\langle \rho(\mathbf{x}) - \rho_p(\mathbf{x}) \rangle \times 10^4$
29	1.164
30	1.157
31	1.153
32	0.690
33	0.499
34	0.458
35	0.425

Table 1: The mean difference $\langle \rho(\mathbf{x}) - \rho_p(\mathbf{x}) \rangle$, magnified by a 10^4 factor, in a grid of 128×128 boxes, each one as the same size.

291 are transient due to the existence of the chaotic saddle in Γ . Figure 4 shows
 292 a high value for the invariant density for specific points along the diagonal
 293 that contains the projection of the synchronized state. These points, which
 294 are in the chaotic saddle, are those associated with the discontinuity of the
 295 local map, β^{-1} , and the respective pre-images. Thus, the probability of a
 296 trajectory in the neighborhood of such points still belongs to the chaotic
 297 saddle is very high. Consequently, the behavior illustrated in Figure 3(a) is
 298 more likely to occur when a trajectory close to \mathcal{S} is near of a discontinuity (or
 299 its pre-images) of the local dynamics. This is the topological explanation for
 300 the non-local instabilities in synchronized state, which supports the heuristic
 301 argument presented in Reference [15]. Direct analysis of our results, espe-
 302 cially those presented in Figures 3 and 4, shows that the divergence between
 303 a typical trajectory and locally stable synchronized state is due strictly to
 304 the existence of UPO's in the unsynchronized state.

305 In conclusion, the analytical conditions for the threshold of transversal
306 stability of the synchronized state of coupled piecewise-linear maps are con-
307 firmed by numerical experiments as long as we observe the following precau-
308 tions: (i) the transient time should be chosen as large as possible, (ii) the
309 choice of initial conditions should be done using a probability distribution
310 which best matches the natural measure of the uncoupled oscillators.

311 Although these computational problems are less likely to occur in cou-
312 pled smooth maps, they do not invalidate the analytical approach to the
313 transversal stability of coupled non-smooth maps, like piecewise-linear ones.
314 Our analysis indicates that results based on linear analysis of stability of the
315 synchronized state may be valid for both smooth and non-smooth local dy-
316 namics. Thus, results as those found in reference [23] are directly extended
317 to piecewise-linear coupled maps. We have used general arguments valid for
318 hyperbolic CML's so as to prove that the local transversal stability of the
319 synchronized state actually implies the synchronization of *all* typical orbits.
320 Finally, since there is the conjecture [16] that the expression (7) is valid for
321 non-hyperbolic systems, we conjecture that our results are valid for networks
322 whose phase space has no structure hyperbolic.

323 **References**

- 324 [1] A. Pikovsky, M. Rosenblum, J. Kurths, Synchronization: A Universal
325 Concept in Nonlinear Sciences (Cambridge Nonlinear Science Series),
326 1st Edition, Cambridge University Press, 2003.
- 327 [2] S. Boccaletti, J. Kurths, G. Osipov, D. L. Valladares, C. S. Zhou, The

- 328 synchronization of chaotic systems, *Physics Reports* 366 (1-2) (2002) 1
329 – 101. doi:10.1016/S0370-1573(02)00137-0.
- 330 [3] K. Wiesenfeld, P. Colet, S. H. Strogatz, Synchronization transitions in a
331 disordered josephson series array, *Physical Review Letters* 76 (3) (1996)
332 404 – 407. doi:10.1103/PhysRevLett.76.404.
- 333 [4] R. Roy, K. S. Thornburg, Experimental synchronization of chaotic
334 lasers, *Physical Review Letters* 72 (13) (1994) 2009 – 2012.
335 doi:10.1103/PhysRevLett.72.2009.
- 336 [5] L. M. Pecora, T. L. Carroll, Synchronization in chaotic sys-
337 tems, *Physical Review Letters* 64 (8) (1990) 821 – 824.
338 doi:10.1103/PhysRevLett.64.821.
- 339 [6] L. M. Pecora, T. L. Carroll, G. A. Johnson, D. J. Mar, J. F. Heagy,
340 Fundamentals of synchronization in chaotic systems, concepts, and ap-
341 plications, *Chaos* 7 (4) (1997) 520–543. doi:10.1063/1.166278.
- 342 [7] L. M. Pecora, Synchronization conditions and desynchronizing patterns
343 in coupled limit-cycle and chaotic systems, *Physical Review E* 58 (1)
344 (1998) 347 – 360. doi:10.1103/PhysRevE.58.347.
- 345 [8] Y. Kawamura, H. Nakao, Y. Kuramoto, Noise-induced turbulence
346 in nonlocally coupled oscillators, *Physical Review E* 75 (3) (2007)
347 036209(17). doi:10.1103/PhysRevE.75.036209.
- 348 [9] S. Raghavachari, J. A. Glazier, Spatially coherent states in fractally
349 coupled map lattices, *Physical Review Letters* 74 (16) (1995) 3297 –
350 3300. doi:10.1103/PhysRevLett.74.3297.

- 351 [10] A. M. Batista, S. E. d. S. Pinto, R. L. Viana, S. R. Lopes, Lyapunov spectrum and synchronization of piecewise linear map lattices
352 with power-law coupling, *Physical Review E* 65 (5) (2002) 056209(9).
353 doi:10.1103/PhysRevE.65.056209.
354
- 355 [11] R. Viana, C. Grebogi, S. de S.Pinto, S. Lopes, A. Batista, J. Kurths,
356 Bubbling bifurcation: Loss of synchronization and shadowing break-
357 down in complex systems, *Physica D* 206 (1-2) (2005) 94 – 108.
358 doi:10.1016/j.physd.2005.05.001.
- 359 [12] R. L. Viana, C. Grebogi, S. E. d. S. Pinto, S. R. Lopes, A. Batista,
360 J. Kurths, Validity of numerical trajectories in the synchronization tran-
361 sition of complex systems, *Physical Review E* 68 (2003) 067204(4).
- 362 [13] C. Anteneodo, S. E. d. S. Pinto, A. M. Batista, R. L. Viana, Analytical
363 results for coupled-map lattices with long-range interactions, *Physical*
364 *Review E* 68 (4) (2003) 045202(4). doi:10.1103/PhysRevE.68.045202.
- 365 [14] A. Katok, B. Hasselblatt, *Introduction to the modern theory of dynam-*
366 *ical systems*, Cambridge University Press, 1996.
- 367 [15] M. Cencini, A. Torcini, Nonlinearly driven transverse synchronization
368 in coupled chaotic systems, *Physica D* 208 (3-4) (2005) 191 – 208.
369 doi:10.1016/j.physd.2005.06.017.
- 370 [16] C. Grebogi, E. Ott, J. A. Yorke, Unstable periodic orbits and the di-
371 mensions of multifractal chaotic attractors, *Physical Review A* 37 (5)
372 (1988) 1711–1724. doi:10.1103/PhysRevA.37.1711.

- 373 [17] Y. Nagai, Y.-C. Lai, Periodic-orbit theory of the blowout bi-
374 furcation, *Physical Review E* 56 (4) (1997) 4031 – 4041.
375 doi:10.1103/PhysRevE.56.4031.
- 376 [18] R. F. Pereira, S. E. de S Pinto, R. L. Viana, S. R. Lopes, C. Grebogi,
377 Periodic orbit analysis at the onset of the unstable dimension variabil-
378 ity and at the blowout bifurcation., *Chaos* 17 (2) (2007) 023131(13).
379 doi:10.1063/1.2748619.
- 380 [19] S. E. d. S. Pinto, J. T. Lunardi, A. M. Saleh, A. M. Batista, Some aspects
381 of the synchronization in coupled maps, *Physical Review E* 72 (3) (2005)
382 037206(4). doi:10.1103/PhysRevE.72.037206.
- 383 [20] W. H. Press, *Numerical Recipes in C*, Cambridge University Press, 1992.
- 384 [21] C. Beck, F. Schogl, *Thermodynamics of Chaotic Systems: An Introduc-*
385 *tion*, Cambridge University Press, Cambridge, 1995.
- 386 [22] Y.-C. Lai, Y. Nagai, C. Grebogi, Characterization of the natural measure
387 by unstable periodic orbits in chaotic attractors, *Physical Review Letters*
388 79 (4) (1997) 649–652. doi:10.1103/PhysRevLett.79.649.
- 389 [23] P. Palaniyandi, G. Rangarajan, Critical lattice size limit for syn-
390 chronized chaotic state in one- and two-dimensional diffusively cou-
391 pled map lattices, *Physical Review E* 76 (2) (2007) 027202(4).
392 doi:10.1103/PhysRevE.76.027202.

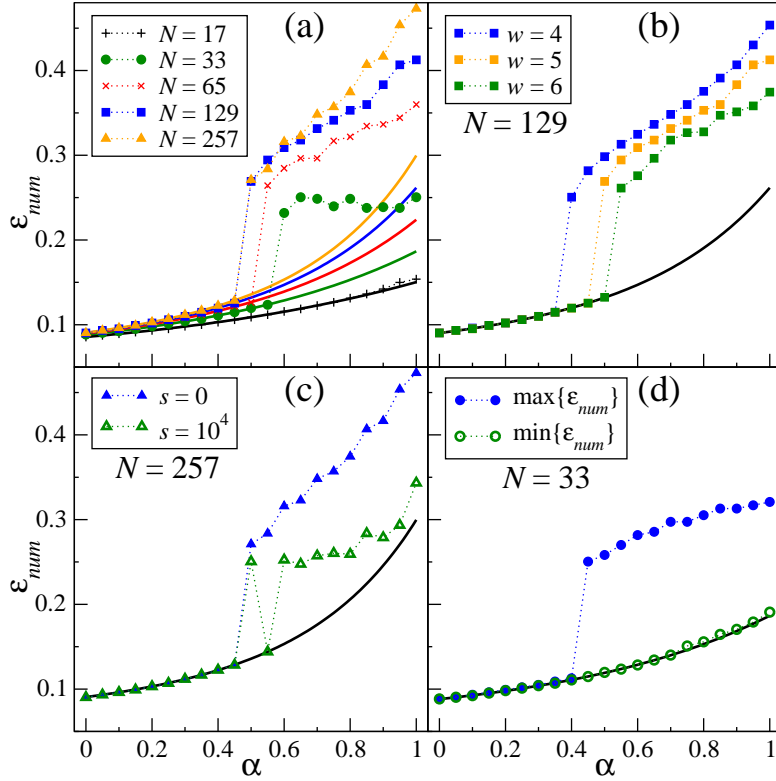


Figure 1: (color online) Values of the coupling strength at the onset of transversal stability loss of the synchronized state, as a function of the effective coupling range. We used $\beta = 1.1$ and (a) different lattice sizes; (b) different transient times T_w , for a fixed lattice size; (c) different distributions of initial conditions, for $N = 257$; (d) different initial conditions, for $N = 33$ and a fixed transient time. The solid lines represent the analytical results from linear transversal stability of the synchronized state.

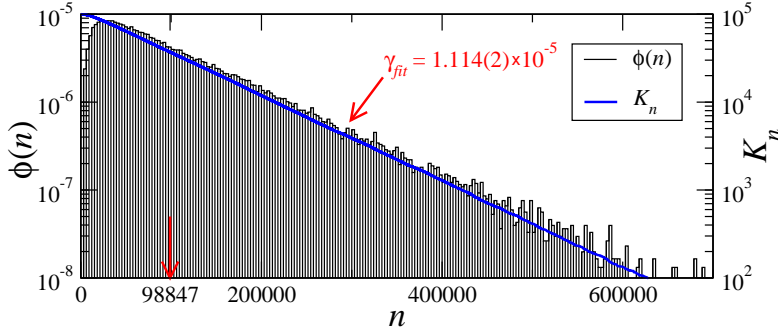


Figure 2: (color online) Line: decay in the number of trajectories in the unsynchronized state for $N = 17$, $\beta = 1.10$, $\alpha = 0.80$ and $\varepsilon = 0.17$ (slightly above the critical curve in Figure 1). Histogram: synchronization times distribution for same lattice parameters. The exponential tail of such distribution is given by the escape rate of the saddle embedded in Γ . The average synchronization time, $\langle n \rangle = 98847$, is approximately given by γ_{fit}^{-1} .

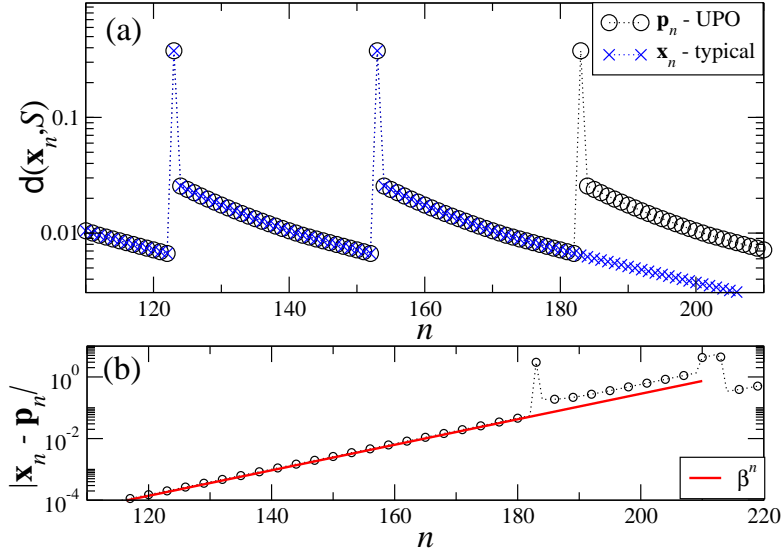


Figure 3: (color online) (a) Series of a typical trajectory, \mathbf{x}_n , in the vicinity of a periodic orbit $\mathbf{p}_n \in \Gamma$. The trajectory follows the periodic orbit for a few periods, and then escapes from the saddle and reach the synchronized state. (b) The distance between the trajectory and the periodic orbit as a function of time n . Trajectory moves away from the UPO at a rate given by the unstable eigenvalue of the orbit.

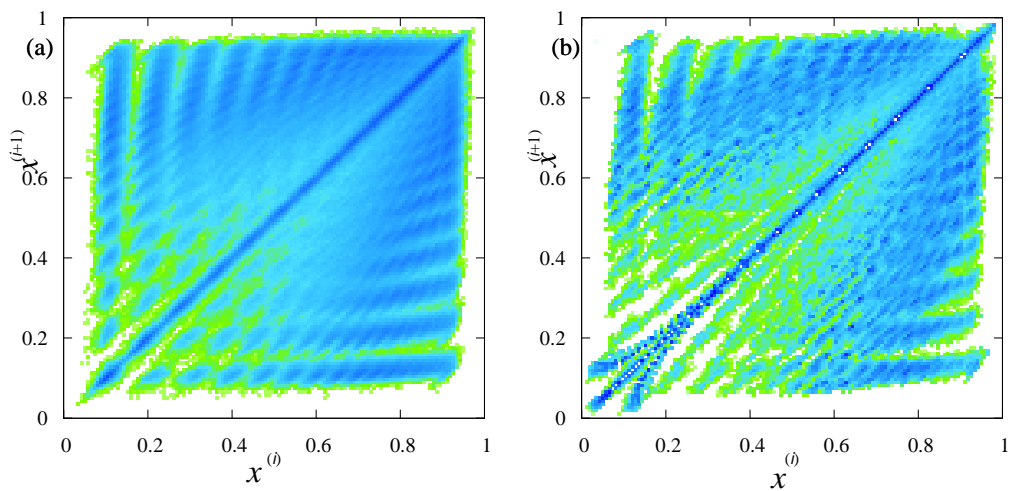


Figure 4: (color online) (a) Density projection of the chaotic saddle that is contained in Γ , for typical trajectories. The color scale indicates the density: the blue color indicates regions most visited and the green color indicates the least visited. (b) Same as previous, but using all unstable orbits with the period less than or equal to 35. The simulations were performed with the following parameters: $N = 17$, $\beta = 1.10$, $\alpha = 0.80$ and $\varepsilon = 0.17$.